



NRC Publications Archive Archives des publications du CNRC

Pore structure and interconnectivity of CdS aerogels and xerogels by hyperpolarized xenon NMR

Pawsey, Shane; Kalebaila, Kennedy K.; Moudrakovski, Igor; Ripmeester, John A.; Brock, Stephanie L.

This publication could be one of several versions: author's original, accepted manuscript or the publisher's version. / La version de cette publication peut être l'une des suivantes : la version prépublication de l'auteur, la version acceptée du manuscrit ou la version de l'éditeur.

For the publisher's version, please access the DOI link below. / Pour consulter la version de l'éditeur, utilisez le lien DOI ci-dessous.

Publisher's version / Version de l'éditeur:

<https://doi.org/10.1021/jp103157t>

The Journal of Physical Chemistry, 114, 31, pp. 13187-13195, 2010-08-12

NRC Publications Record / Notice d'Archives des publications de CNRC:

<https://nrc-publications.canada.ca/eng/view/object/?id=4601cacd-09be-4467-82ec-1e7011c292cf>

<https://publications-cnrc.canada.ca/fra/voir/objet/?id=4601cacd-09be-4467-82ec-1e7011c292cf>

Access and use of this website and the material on it are subject to the Terms and Conditions set forth at

<https://nrc-publications.canada.ca/eng/copyright>

READ THESE TERMS AND CONDITIONS CAREFULLY BEFORE USING THIS WEBSITE.

L'accès à ce site Web et l'utilisation de son contenu sont assujettis aux conditions présentées dans le site

<https://publications-cnrc.canada.ca/fra/droits>

LISEZ CES CONDITIONS ATTENTIVEMENT AVANT D'UTILISER CE SITE WEB.

Questions? Contact the NRC Publications Archive team at

PublicationsArchive-ArchivesPublications@nrc-cnrc.gc.ca. If you wish to email the authors directly, please see the first page of the publication for their contact information.

Vous avez des questions? Nous pouvons vous aider. Pour communiquer directement avec un auteur, consultez la première page de la revue dans laquelle son article a été publié afin de trouver ses coordonnées. Si vous n'arrivez pas à les repérer, communiquez avec nous à PublicationsArchive-ArchivesPublications@nrc-cnrc.gc.ca.



Pore Structure and Interconnectivity of CdS Aerogels and Xerogels by Hyperpolarized Xenon NMR

Shane Pawsey,^{*,†,§} Kennedy K. Kalebaila,[‡] Igor Moudrakovski,[†] John A. Ripmeester,[†] and Stephanie L. Brock^{*,‡}

Steeacie Institute for Molecular Sciences, National Research Council of Canada, Ottawa, Ontario, Canada K1A 0R6, and Department of Chemistry, Wayne State University, Detroit, Michigan 48202

Received: April 7, 2010; Revised Manuscript Received: June 30, 2010

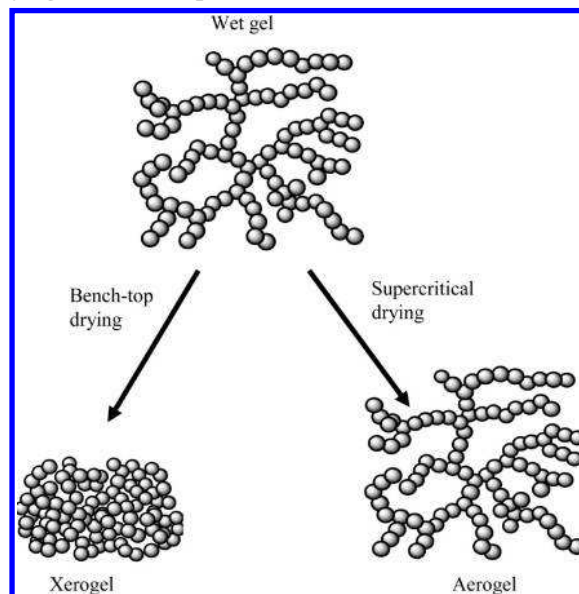
Metal chalcogenide aerogels and xerogels are unique materials that combine semiconducting nanostructures with porosity and are thus of interest for photocatalysis and sensing. To assess the feasibility for applications dependent on molecular transport, the pore structure and interconnectivity in CdS aerogels and xerogels were probed by a combination of conventional techniques and hyperpolarized (HP) ^{129}Xe NMR. HP ^{129}Xe NMR of the aerogels was consistent with two distinct types of accessible pores (adsorption sites), and 2-D EXSY NMR data suggest that these are connected. In contrast, a single resonance of low intensity with a temperature dependence consistent with the dissolution of Xe within a polymer matrix, that is, transport facilitated at high temperatures due to chain motion, is observed in xerogels. ^{13}C NMR and thermal gravimetric analysis data reveal the presence of residual organics in both xerogels and aerogels, but a relatively higher proportion in the former, due, in part, to the surfactant used in their preparation. These data, combined with the absence of any meaningful adsorption isotherm for N_2 at 77 K (where limited thermal chain motion precludes gas adsorption) are consistent with a dynamic blocking of the xerogel pores. The results reveal the important role of residual organics and drying regimens on the accessibility of pores in metal chalcogenide gel architectures.

Introduction

Porous nanostructures are strategic materials for catalysis, separation and storage of gases, and many other applications.^{1,2} Most of these applications are dependent on the ability of gases to percolate from one pore to the next; that is, they make use of an interconnected pathway. Moreover, for facile mass transport through the matrix, the pore sizes should be in the meso regime (2–50 nm). Colloidal and/or polymeric gel networks embody these desirable features, and thus, their solid-state analogs, aerogels and xerogels, are extensively studied. Aerogels are dried gels that retain the porosity of the wet gel from which they are formed. Typically, to preserve the structure, supercritical drying is required, and the resultant aerogels are characterized by a broad range of pores that extend from the microporous (<2 nm) to mesoporous (2–50 nm) to macroporous (>50 nm) regimes (Scheme 1). In contrast, wet gels dried under ambient conditions or under vacuum undergo compaction, yielding a more dense xerogel (Scheme 1). In both aerogels and xerogels, an open cell structure is presumed, thereby providing access to the active surface from the gas phase or in solution for the reaction/deposition of materials.

Traditionally, aerogels are based on oxide frameworks (typically silica), which limits the properties that can be accessed. In particular, aerogels based on direct band-gap semiconductor materials with optical properties extending into the visible and IR have been lacking. Recently, a new class of aerogels and xerogels based on metal chalcogenides (in lieu of oxides) has been developed.^{3–11} These semiconducting metal

SCHEME 1: Pictorial Representation of the Effect of Drying on the Compactness of a Generic Dried Gel



chalcogenide aerogels and xerogels are essentially macroscopic monoliths of quantum dot assemblies that exhibit tunable optical band gaps and narrow photoluminescence emissions. The effective band gap of the quantum confined system depends sensitively on the chemical constituents of the aerogel, the primary particle size, and the network density. These properties, combined with the porous architecture, make them uniquely suited for a range of potential applications, including photocatalysis and optical sensing.^{12–20} Additionally, related chalcogenides prepared from condensation of molecular anionic clusters and

* To whom correspondence should be addressed. E-mail: shane.pawsey@brucker-biospin.com (S.P.), sbrock@chem.wayne.edu (S.L.B.).

[†] Steacie Institute for Molecular Sciences, National Research Council of Canada.

[‡] Wayne State University.

[§] Present address: Bruker Biospin Corporation, Billerica, MA.

ions have been shown to be potent materials for selective adsorption of heavy ions from solution as well as selective separation of small molecules in the gas phase.^{21,22} However, a detailed appreciation of the size and connectivity of pores in chalcogenide aerogels and xerogels is needed to effectively exploit these materials.

Common methods for probing pore size, pore volume, and surface area include gas sorption isotherms, pycnometry, and mercury porosimetry. However, such classical methods are time-consuming, based on a number of theoretical assumptions and often require high pressures (e.g., mercury porosimetry) that may be detrimental to the pore wall structure.²³ Additionally, although the determination of surface areas and pore sizes by the Brunauer, Emmett, and Teller (BET) method and Barret, Joyner, and Halenda (BJH) methods is routinely employed, the two techniques do not provide information on the connectivity of the pores in the network and reflect the structure at low temperatures (77 K). Thus, there is a need to explore other methods that would provide temperature-dependent details on the porous network structure in terms of free or obstructed pathways, important considerations for applications that require mass transfer.

¹²⁹Xe nuclear magnetic resonance (NMR) has developed into a powerful technique in the study of porous solids^{24–27} because the large chemical shift range of ¹²⁹Xe is heavily influenced by local environmental and chemical factors, such as the profile and size of void spaces and the nature and concentration of any coadsorbed molecules. Compared with other techniques (TEM, gas adsorption isotherm measurements, SAXS) that, in principle, provide information on pore size, volume, and surface area, ¹²⁹Xe NMR spectroscopy has the advantage of probing the connectivity and uniformity of the pores at a range of temperatures, as well as the dynamic motion of any soft-material components, information that may be difficult to obtain with the other techniques. As such, ¹²⁹Xe NMR spectroscopy has been used for characterization of porous systems ranging from zeolites,^{28,29} aluminophosphates,^{30–32} polymers,^{33–36} and organic zeolite isomorphs³⁷ to biological systems.³⁸

In a limited number of studies, ¹²⁹Xe NMR has been employed for the characterization of silica and organic aerogels or xerogels.^{39,40} Several research groups have reported evidence linking xenon chemical shifts to xenon occluded within porous aerogels and xerogels.^{39–41} In silica xerogels, chemical shifts between 95 and 120 ppm are observed, consistent with a large degree of contact between Xe and the pore walls and thus microporosity.⁴¹ In a silica aerogel, one group observed from a combination of Xe NMR and spectroscopic imaging that areas devoid of Xe represented regions in the aerogel where there was extensive pore collapse, whereas areas with a high density of Xe were ascribed to more open spaces within the aerogels.⁴⁰ Moreover, the peaks were shifted upfield relative to the xerogels (20–60 ppm), consistent with pores in the meso regime. Studies on organic resorcinol–formaldehyde aerogels have shown that, on the millisecond time scale, exchange is facile between free Xe and Xe within micro- or mesopores.³⁹ Additionally, on the same time scale, an exchange occurs between micropores (with chemical shifts of 140 ppm) and mesopores (with chemical shifts of 85–100 ppm), showing that they are intimately connected and hierarchical.³⁹

In this paper, we have applied ¹²⁹Xe NMR to assess the pore structure and interconnectivity of chalcogenide aerogels and xerogels for the first time, for the specific case of CdS. We detail the interaction of Xe gas with CdS aerogels and xerogels, highlight the differences in observed chemical shifts and their

temperature dependence due to the nature of pores in the dried gels and the presence of occluded organics, and probe the interconnectivity of the pores by 2-D EXSY NMR. These data are discussed in the context of relevant ¹³C NMR MAS, nitrogen physisorption, and thermal gravimetric analysis (TGA) data, and models are proposed for the macroscopic structure of CdS aerogels and xerogels and compared to traditional silica-based materials. Finally, the suitability of the CdS pore–matter nanostructures for applications that exploit the optoelectronic properties of the matter network and the transport properties of the pore network are discussed.

Experimental Section

Materials. Cadmium nitrate (Cd(NO₃)₂), sodium sulfide (Na₂S), dioctyl sulfosuccinate sodium salt (AOT), 4-fluorobenzenethiol (FPhSH), and triethylamine (TEA) were all purchased from Aldrich and used as received. All solvents used were of pure grade.

Synthesis of CdS Nanoparticles and Resultant Aerogels. Cadmium sulfide nanoparticles were prepared following a modified procedure from Gacoin and co-workers.^{42–44} In a typical synthesis, 101 mL of an aqueous solution of 0.15 M Cd(NO₃)₂ and Na₂S solutions were placed into separate round-bottom flasks containing 1899 mL of 0.56 M AOT in *n*-heptane. After stirring the colorless solutions for 2 h, the S²⁻ micellar solution was cannulated into the Cd²⁺ micellar solution and stirred for 24 h, leading to the formation of yellow CdS nanoparticles. Thiolate capping of the CdS nanoparticles was achieved by the addition of 9 mL of the complexing agent, FPhSH, followed by the addition of 11 mL of TEA to adjust the pH of the solution to 11.2. After stirring for 4 h, the capped CdS nanoparticle precipitate was isolated by centrifugation, followed by washing four times with *n*-heptane. The precipitate was then dispersed in 100 mL of acetone.

To the 100 mL of the CdS sol in a centrifuge tube was added 2 mL of 3% H₂O₂ to initiate gelation. The mixture was shaken vigorously, then allowed to sit undisturbed for gelation. The wet gels thus formed were aged for 3 days before performing solvent exchange three times with acetone and transferring to an SPI-DRY model critical point dryer, where they were subsequently exchanged and immersed in CO₂(l) over 8 h. The CO₂(l)-exchanged gels were dried under supercritical conditions by raising the dryer temperature to 39 °C and maintaining this temperature for 45 min, followed by venting of CO₂ gas over 45 min to obtain aerogels. CdS xerogels were prepared by simple evaporation of the wet gels left on the benchtop. Because of the large sample size requirements for solid-state NMR, we combined the products from several reactions together to create an “average” sample upon which all characterization was performed.

Characterization. The structural and morphological characteristics of CdS nanoparticles, xerogels, and aerogels were characterized by powder X-ray diffraction (PXRD) and transmission electron microscopy (TEM). Samples for PXRD were prepared by placing a fine powder of the dry gels on a quartz (0001) low background holder previously smeared with silicone grease. The data were collected from 10–70° (2θ) at a voltage of 40 kV and current of 150 mA using a Rigaku RU 200B diffractometer equipped with a copper rotating anode source. The TEM micrographs were recorded on a JEOL 2010 analytical electron microscope using a carbon-coated copper grid as a sample holder. The TEM samples were prepared by placing a drop of a sonicated acetone solution of aerogel or xerogel on the grid and then drying in a vacuum desiccator.^{3,4,8}

The surface area and pore size distributions of the gels were determined from nitrogen adsorption/desorption isotherms acquired at 77.2 K using a 30 s equilibrium interval on a Micromeritics ASAP 2010 porosimeter. The surface area was computed by the BET (Brunauer–Emmett–Teller) model, whereas the average pore size and cumulative pore volumes were obtained from the BJH (Barret–Joyner–Halenda) model.⁴⁵ Adsorbed molecules were removed by degassing the samples at 100 °C for 24 h prior to analysis. Thermal gravimetric analysis (TGA) data were collected on a PerkinElmer Pyris 1 TGA instrument, under a nitrogen atmosphere, by heating the samples isothermally at 100 °C for 16 h, then heating to 800 °C at a rate of 20 °C/min. A second set of data was acquired on a TA Instruments TGA/DSC (2050) to 500–580 °C at a rate of 5 °C/min.

Solid-state ¹³C MAS (magic-angle spinning) NMR experiments were performed on a Bruker DSX-400 spectrometer (magnetic field = 9.4 T, ¹³C resonance frequency = 100 MHz) using a variable-temperature double resonance probe. Cross-polarization with high power ¹H decoupling was used to obtain ¹³C spectra of the aerogel and xerogel samples. The samples were loaded into 4 mm rotors and heated at 50 °C under a flow of He overnight prior to data collection. Samples were spun at 12.5 kHz and 18 600 transients were collected for the aerogel sample and 15 500 for the xerogel, while a contact time of 2 ms and a repetition delay of 4 s were employed.

¹²⁹Xe NMR measurements were performed on the same instrument using a continuous flow of hyperpolarized (HP) Xe. The samples (ca. 60–80 mg) were prepared by pouring the powdered aerogel or xerogel into a glass cell that lies within the NMR coil. The continuous flow polarizer apparatus used for the production of HP Xe was similar in design to that previously reported^{46,47} and employed an 80 W CW diode laser from Coherent operating at a wavelength of 795 nm as the source of optical excitation. A gas mixture of xenon–helium–nitrogen with a volume composition of 1%/96%/3% was used for all HP xenon experiments, and the flow rate was set in the range of 140–160 cc/min, monitored with a Vacuum General flow controller (model 80-4). The polarization of the cell (new) was in the range of 12–15% and is known to decrease with time. The stream of HP Xe gas was delivered from the cell through plastic tubing directly to the CdS aerogel or xerogel sample, which was confined within the 5 mm coil of a modified static Bruker NMR probe with the use of glass wool plugs that allowed for the flow of gas. Sixty-four scans were recorded with a repeat time of 2 s. The T₁ of dilute Xe within the sample is unknown but is effectively shorter than the repeat time, as no saturation is observed under experimental conditions. The ¹²⁹Xe NMR chemical shifts were referenced to xenon gas extrapolated to zero pressure. Variable-temperature NMR experiments over the range of 173–353 K were performed using a Bruker BVT3000 temperature controller. 2D-EXSY spectra were obtained using the standard sequence described elsewhere.^{48–53}

The enthalpy of adsorption (ΔH_{ads}) and ¹²⁹Xe chemical shift characteristic of the surface (δ_{s}) were extracted by fitting the observed chemical shift (δ) as a function of temperature (T); see eq 1.⁵⁴ In this equation, K_0 is the pre-exponent in the Henry equation,⁵⁴ D is the channel diameter, and R is the universal gas constant. The validity of this method has been demonstrated for a wide variety of silica materials, including those with ordered or random pore networks, and with micropores and/or mesopores.⁵⁵

$$\delta = \delta_{\text{s}} \left(1 + \frac{D}{4K_0RT^2 \exp\left(\frac{\Delta H_{\text{ads}}}{RT}\right)} \right)^{-1} \quad (1)$$

Results and Discussion

Morphology, Structure, and Composition of CdS Aerogels and Xerogels. The formation of aerogels or xerogels from wet CdS gels is a function of the drying conditions. When the wet gels are dried from supercritical CO₂, where there is no liquid/gas interface (no surface tension), an aerogel is achieved, wherein the 3-D network of the wet gel is retained; see Scheme 1. On the other hand, the large shrinkage of the network in the xerogel is due to the capillary forces exerted by the meniscus of the pore liquid as the solvent evaporates from the surface of the gel under ambient conditions.¹ The morphological consequences are readily apparent in the TEM. Figure 1a shows a representative micrograph of the CdS aerogel, revealing a network of colloidal nanoparticles connected in a random fashion with pores evident. On the other hand, xerogels showed a much denser network of colloidal particles, with fewer apparent pores (Figure 1b). The purity and structural phase of the CdS aerogels and xerogels was probed by PXRD (Supporting Information), and all observed peaks match the diffraction patterns of the cubic CdS phase, consistent with prior results.^{3,4}

To determine if organic moieties present in the synthesis are retained in the dried gels, ¹³C CPMAS data were acquired. Data for the CdS xerogel and aerogel are shown in Figure 2 and display several peaks in the range of 10–180 ppm, indicative of a significant quantity of residual organics. Although the spectral features are similar for each, there is a much better signal-to-noise (S/N) ratio for the xerogel spectrum relative to that of the aerogel, consistent with a larger quantity of organic matter in xerogels relative to aerogels. These are most likely to be residual AOT surfactant, thiolate capping groups (FPhS⁻), or TEA. With this in mind, peaks in the region of 60–70 and 160–180 ppm can be attributed to C–O and C=O groups, respectively, of the AOT surfactant and peaks between 10 and 40 ppm can be attributed to CH₂ and CH₃ groups of AOT and/or TEA.⁵⁶ Peaks in the 115–140 ppm are consistent with aromatic C=C groups, as is found in FPhS⁻. The C–S and C–F peaks of FPhS⁻ would be expected to occur around 160 ppm but could be challenging to observe with a 2 ms contact pulse due to a relatively large separation from ¹H spins and also may overlap with peaks due to the C=O groups from AOT. However, ¹⁹F MAS NMR (Supporting Information) reveals peaks between 30 and 45 ppm, attributable to FPhS⁻. Thus, despite considerable washing, the gels appear to retain considerable quantities of all the organic species to which they have been exposed during their synthesis.

To quantify the amount of residual organic species in the aerogels and xerogels, TGA analysis was performed under an inert flowing atmosphere, and the results are shown in Figure 3. After heating the samples at 100 °C for over 12 h, the aerogel samples showed a 2% weight loss, whereas the xerogel showed a relatively higher weight loss of 6%. When heated up to 800 °C, the samples became discolored, turning from the characteristic yellow color of the CdS gels to a black, opaque material. This is likely due to thermal decomposition of the residual organics observed in the ¹³C NMR. CdS aerogels lose a further 29 wt % of material up to 700 °C, whereas the xerogel counterpart loses an additional 38 wt %. A second set of measurements conducted on a different instrument and using a different temperature profile showed a similar trend: a 23% loss

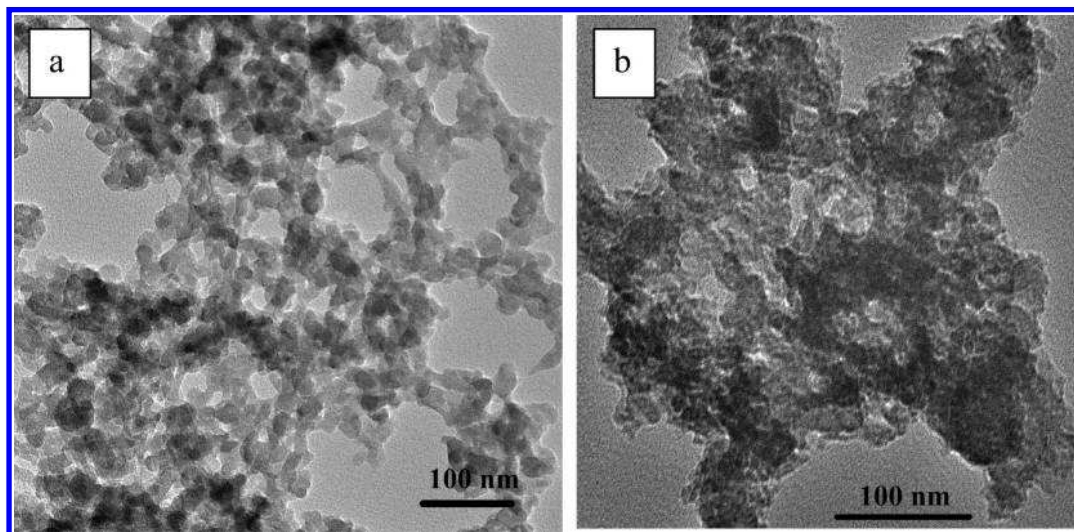


Figure 1. TEM micrographs of (a) a CdS aerogel and (b) a CdS xerogel.

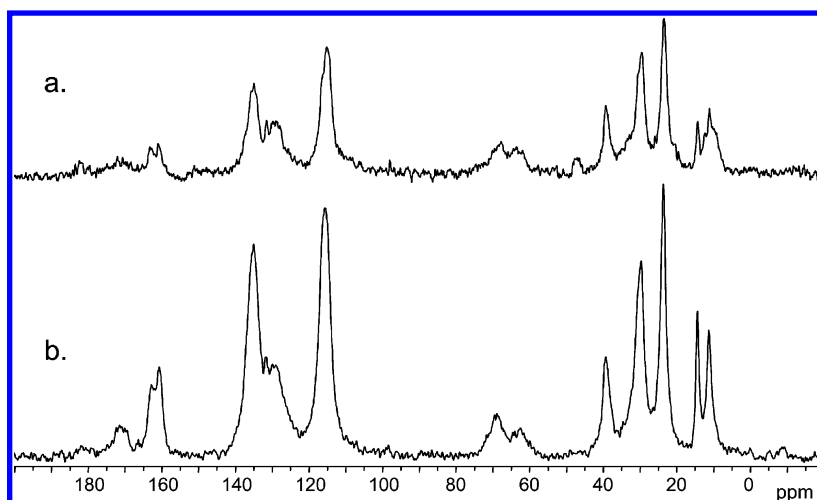


Figure 2. ^{13}C CPMAS NMR spectrum of a CdS (a) aerogel and (b) xerogel. The scale at the bottom corresponds to both spectra.

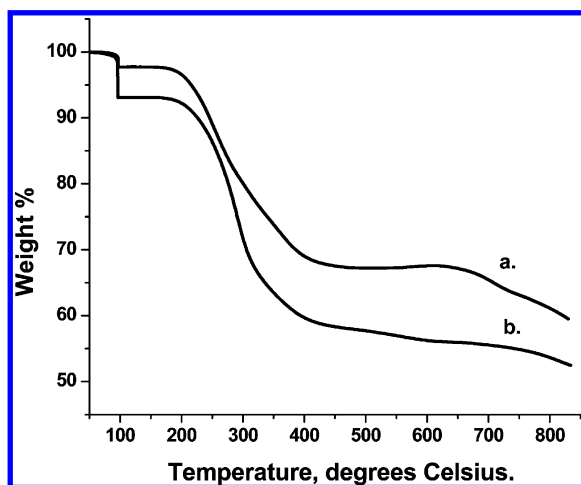


Figure 3. Thermal gravimetric analysis curves of (a) a CdS aerogel and (b) a CdS xerogel. The samples were held at 100 °C for 16 h to ensure the complete removal of water.

for the aerogel and a 31% loss for the xerogel. Moreover, the xerogel samples appear nearly black after heating to 500 °C, whereas the aerogels show no corresponding color change, even up to 580 °C. This is consistent with pyrolysis of organics in the xerogels at lower temperatures than in the aerogels, which may be exacerbated by the small pore size. In all cases, the

weight losses show that xerogels contain more volatile matter than aerogels. The fact that the aerogels appear to be relatively cleaner than the xerogels may be ascribed to the extra washing of the gel achieved during the CO_2 exchange step prior to supercritical drying and aerogel formation. The combined ^{13}C NMR and TGA data show that, despite the best efforts to wash off byproducts and excess ligands before drying, there is always residual ligand adsorbed to the surface. The effect of these residual AOT and fluorobenzenethiolate groups will be highlighted by differences between the xerogel and aerogel porosity, as reflected in the N_2 physisorption and Xe NMR data.

Probing the Pore Structure in CdS Aerogels by N_2 Physisorption and Xe NMR. The surface area, average pore size, and cumulative pore volumes for the CdS aerogels probed by N_2 physisorption at 77 K were found to be 240 m^2/g , 11.8 nm, and 0.92 cm^3/g , respectively. The aerogel samples show a type IV isotherm combined with a type H1 hysteresis loop, as shown in Figure 4, suggesting the presence of cylindrical mesopores in the samples.^{45,57} Pore size analysis by BJH modeling of the nitrogen sorption data shows that the CdS aerogels produced here have a size distribution ranging from 5 to 90 nm (Figure 4, inset) with a maximum at ~ 23 nm. This distribution is consistent with the observed random pore sizes in the TEM images of the aerogels.

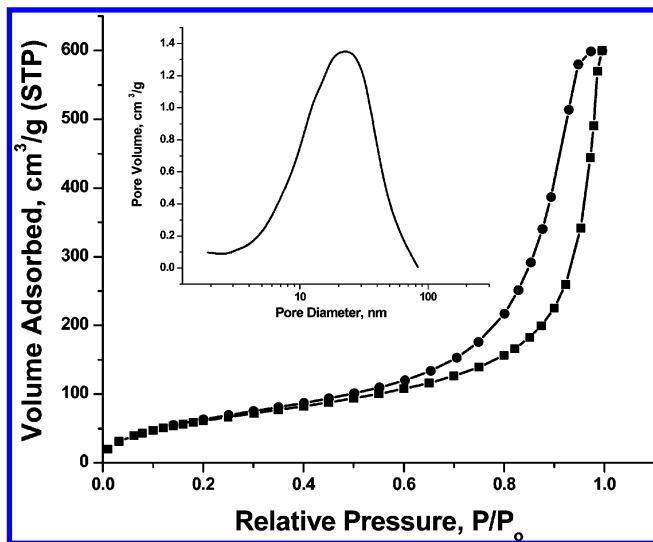


Figure 4. Adsorption/desorption isotherm for a CdS aerogel previously degassed at 100 °C for 24 h. The inset shows the distribution of porosity in the sample.

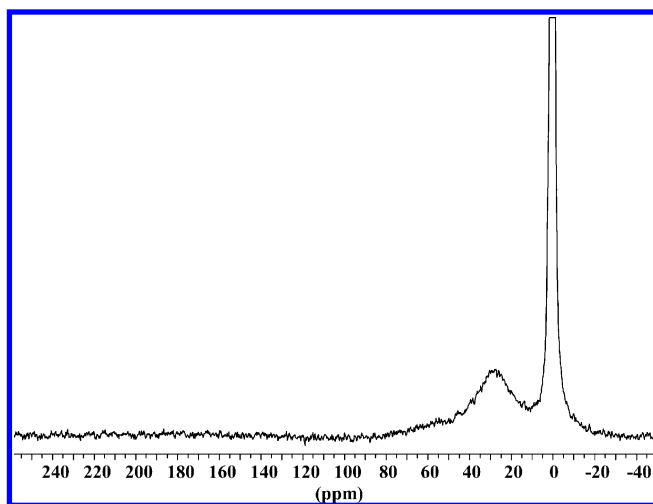


Figure 5. HP ^{129}Xe NMR spectrum of xenon in a CdS aerogel at 293 K.

Although the N_2 physisorption data can tell us something about the low-temperature porosity of a system, it is not possible to discern the temperature-dependent characteristics or the dynamics of molecule–pore interactions. Accordingly, HP ^{129}Xe and ^{129}Xe 2-D EXSY experiments were conducted. The room-temperature (293 K) continuous flow HP ^{129}Xe spectrum of the CdS aerogel (Figure 5) shows a strong sharp signal for free, or unadsorbed (not interacting with the CdS aerogel) xenon, which is observed at 0 ppm, and at least two other broad peaks centered at approximately 55 and 27 ppm (more easily resolved at low temperatures; see Figure 6). These correspond to xenon gas adsorbed in void spaces of different dimensions within the aerogel matrix, with the breadth indicative of a chemical shift distribution from xenon gas sampling a range of similar environments at a rate slower than the NMR experiment time scale. The chemical shift range (27–55 ppm) over which these peaks are located is generally indicative of the void spaces being in the mesopore size regime,⁵⁵ in accordance with the nitrogen physisorption data.

The spectra recorded at variable temperatures, shown in Figure 6, run from 173 to 293 K in 15 K intervals. Higher temperatures were not probed due to concerns over pore collapse. The free gas peak stays constant at 0 ppm throughout

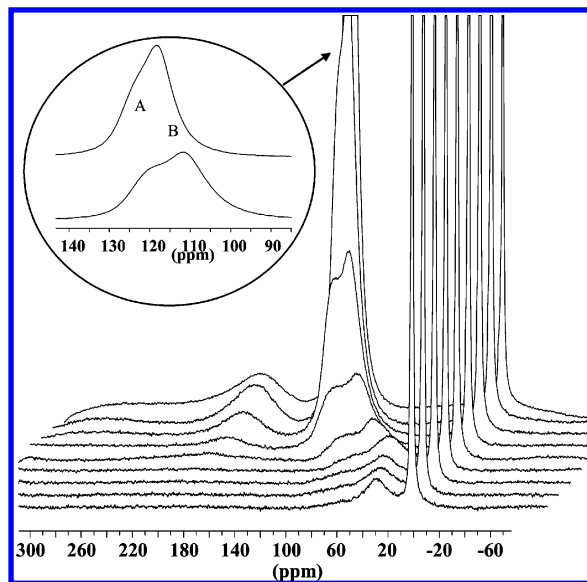


Figure 6. HP ^{129}Xe NMR variable-temperature spectra of xenon in a CdS aerogel between 173 and 293 K recorded every 15 K, with 293 K in the foreground. The inset displays the adsorbed Xe signals A and B at 173 and 188 K, from top to bottom.

the variable-temperature run, but the adsorbed xenon peaks move from smaller to larger chemical shifts with decreasing temperature, indicative of a slower exchange between the adsorbed xenon and free gas. Also, the signal intensity is much greater for the adsorbed peaks due to the greater concentration of xenon within the pores as the temperature was lowered. At 173 K, the adsorbed signals overlap with a maximum at 118 ppm and a shoulder on the downfield side (ca. 122 ppm) corresponding to the second void environment. The proximity of the chemical shifts between the two void spaces indicates that xenon is sampling similar area environments. The additional broad signal observed downfield (~ 190 ppm) at lower temperatures could be attributed to smaller pores that are only sampled when the temperature is low enough. The chemical shift of this signal changed relatively little with increasing temperature; however, the signal became much broader until it blended into the baseline and was no longer observable at temperatures above 248 K. At higher temperatures, the xenon exchanges too rapidly or the concentration of xenon is too dilute for a signal to be observed.

Using the variable-temperature continuous flow HP ^{129}Xe NMR results, the diameter of the void spaces has been estimated for a variety of silica materials, with both ordered, monodisperse pore structures and random, polydisperse pore structures.⁵⁵ This is achieved by fitting the chemical shift as a function of temperature to yield the heat of adsorption of xenon from which the diameter of the void spaces can be estimated using an empirical chemical shift–pore size correlation geometrical model.^{54,58} We have applied this model to the CdS aerogels. Figure 7 shows the plot of the xenon chemical shift as a function of temperature for the two signals with lower chemical shifts (the broad signal at higher shift is omitted because its position is practically temperature-independent). The calculated values for the enthalpy of adsorption, void space diameter, and the chemical shift of xenon interacting solely with the aerogel are recorded in Table 1. The effect of xenon–xenon interactions at such a dilute concentration is negligible and becomes important only at very low temperatures when the gas approaches condensation. This phenomenon is observed in the chemical shift versus temperature curve as a plateau and, for

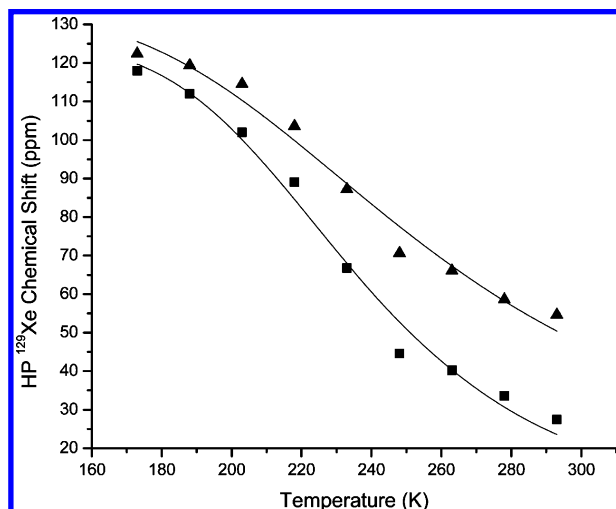


Figure 7. Plot of the HP ^{129}Xe chemical shift as a function of temperature for xenon in CdS nanoparticle aerogels. The solid lines are best fit traces from eq 1. The triangles refer to Peak A of Figure 6 and the squares to Peak B.

TABLE 1: Chemical Shift, Heats of Adsorption, and Pore Diameter Data for the Two Peaks Probed in the CdS Aerogel Sample^a

sample	δ_s (ppm)	ΔH_{ads} (kJ/mol)	D_c (nm)
aerogel peak A	133	13	2
aerogel peak B	125	18	3

^a Data are based on a single sample, and precision is reflected in the number of significant figures reported.

the present samples, is only operative at temperatures below 180 K (Figure 7). The enthalpies of adsorption were determined from eq 1 to be 13 and 18 kJ/mol for the higher (A) and lower (B) chemical shift signals, respectively. The corresponding void space diameters, sampled by the xenon gas, were estimated to be on the order of 2 nm for (A) and 3 nm for (B). The average pore diameter estimated from the BJH model (assuming cylindrical pores) is approximately 5 times larger than that estimated by HP ^{129}Xe NMR. The origin of the large difference is unclear, but it is worth noting that CdS is chemically very different from silica and is, therefore, likely to have different Xe adsorption characteristics. Moreover, the residual organic functionalities on the surface are also likely to contribute to the adsorption enthalpy. Indeed, ^{129}Xe NMR studies of thiophenol-capped CdS nanoparticles revealed similar values to ours (ca. 20 kJ/mol), indicating that our values are reasonable.⁵⁹ Unfortunately, in this prior study it was not clear whether the adsorption was occurring on thiophenol-capped surfaces or in particle cavities or voids between the cavities. Alternatively, the discrepancy we observe in pore size may arise from sampling of the space between the powdered aerogel grains, an effect that has been noted in mesoporous silica materials with submicrometer grain sizes and which is known to result in the broadening and a shift of the ^{129}Xe NMR line upfield, thereby resulting in an underestimation of pore size.⁵⁵ A similar effect has been noted in silica aerogels.⁴⁰ Regardless, the nitrogen physisorption and ^{129}Xe NMR data are consistent with the conclusion that the CdS aerogels consist largely of mesopores (i.e., pores of 2–50 nm), an advantageous pore size regime for molecular transport through the matrix.

Xe 2-D EXSY data were acquired for the CdS aerogel in order to determine the connectivity of the pores and the relative accessibility of the two discernible pore environments (A and

B) to xenon gas. In general, when the exchange time becomes sufficiently long to allow for an exchange to occur between A and B, off-diagonal peaks are expected to arise in the 2-D spectrum. As shown in Figure 8 for data acquired at 233 K (the highest temperature where the A and B are well-resolved), the lack of an off-diagonal signal intensity for mixing times of 1 μs or less indicated that there is no exchange at this time scale between the adsorption sites with larger and smaller chemical shifts (A and B, respectively) or between the free Xe gas and the adsorption sites. At 2 ms, off-diagonal signal intensity correlating adsorption sites A and B is observed, showing that an exchange between the two sites occurs on this time scale, whereas an exchange between B and the free gas does not occur until 10 ms. An exchange between peak A and the free gas is finally observed at 50 ms. At room temperature, it was qualitatively observed that exchange started at shorter times than at 233 K, but like the observation at lower temperatures, an exchange between adsorption site B and the free gas occurs *before* an exchange between A and the free gas. This implies that there is only a small barrier to exchange between the adsorption sites and the barrier to exchange with the free gas is notably larger, especially in the case of adsorption site A. Peak A being less accessible to the free gas region than peak B indicates that free xenon likely has to travel through site B to arrive at site A. This reinforces the likelihood that, of the two observed sites accessible to Xe, A is buried deeper than B, has a narrower opening restricting access, or, most likely, is linked to the free gas region through B.

Probing the Pore Structure in CdS Xerogels by N_2 Physisorption and Xe NMR. In contrast to the aerogels, it was not possible to generate a meaningful nitrogen sorption isotherm for CdS xerogels, suggesting a lack of pores, the occlusion of pores, or the existence of very small pores that become quickly saturated with nitrogen gas. This is surprising because, although TEM of the xerogels shows that this network is more compact than that of the aerogel (Figure 1), mesopores are evident and should be accessible to N_2 . Moreover, previous physisorption studies on CdS xerogels conducted in our lab suggest that, at least in some samples, good N_2 isotherms can be obtained and reflect reasonable surface areas (ca. 50 m^2/g).^{3,8}

As a more comprehensive probe of the void space of the CdS xerogels, HP ^{129}Xe NMR experiments were conducted. Figure 9 shows a signal for adsorbed xenon close to the free gas (0 ppm) at low temperatures (173 K). This signal likely corresponds to xenon adsorbed in a very large void space, possibly an indentation or puddle-like feature on the surface of the xerogel, capable of exchanging rapidly with the free xenon gas. The adsorbed xenon signal closest to 0 ppm exchanges increasingly rapidly as the temperature climbs, resulting in the gas spending more time in the free gas state, on average, leading to a chemical shift that matches the free gas signal. A second peak corresponding to adsorbed xenon near 200 ppm emerges above 173 K. This peak behaves in an unexpected manner, with a chemical shift that increases as the temperature rises, then reverses and changes to smaller chemical shifts at temperatures above 248 K. The large chemical shift cannot be explained by condensed or liquid xenon, as the temperature was too warm. However, this peak falls into a range that is associated with either very small (microporous) voids^{55,60} or what is frequently observed for xenon dissolved in a polymer.^{61,62} Given the thermal behavior of the peak, the latter is more likely. It appears in this situation that xenon has dissolved into the residual organic component present in the CdS xerogels, and thus, the chemical shift behavior may be related to the dynamics of the surfactant (AOT)

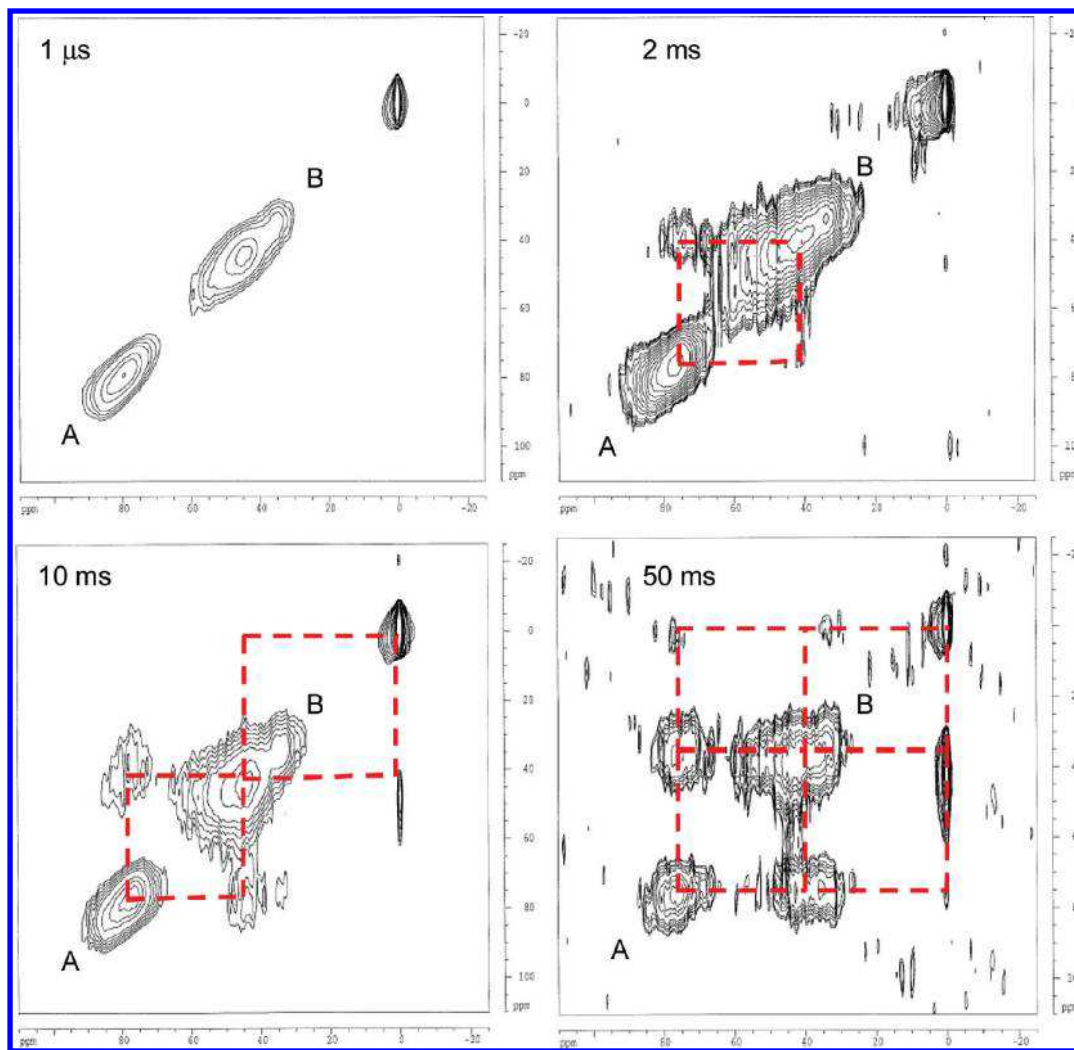


Figure 8. Two-dimensional EXSY HP ^{129}Xe NMR spectra of xenon in a CdS aerogel with mixing times of 1 μs , 2 ms, 10 ms, and 50 ms recorded at 233 K.

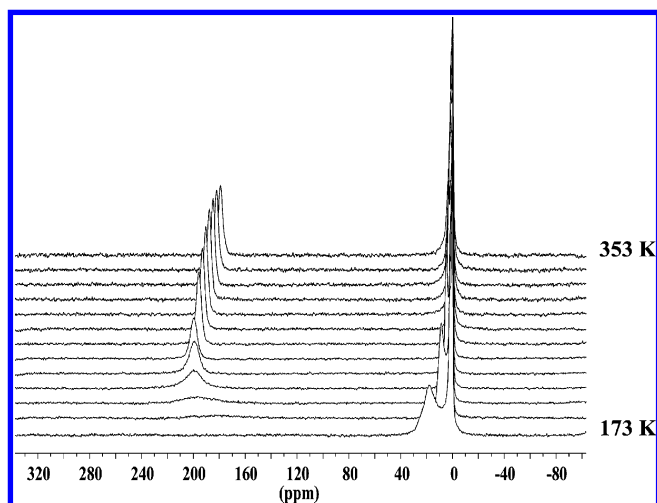


Figure 9. HP ^{129}Xe NMR variable-temperature spectra of xenon in a CdS xerogel between 173 and 353 K, recorded every 15 K.

chains. At the low-temperature end, the dynamics are too slow for the xenon to dissolve in and out of the organic capping groups, or to sample the available environment rapidly, resulting in a broad peak representing a distribution of shifts. As the temperature is raised, the organic chains become more dynamic and the xenon is able to slowly dissolve into and among the organic layer.

Although our failed attempts to acquire nitrogen physisorption data at 77 K suggested a complete lack of accessible space in the CdS xerogels reported here, the NMR data suggest that there is space, but access is hindered by soft matter motions and facilitated at higher temperatures where these motions are more dynamic. These most likely arise from AOT and residual thiolate capping groups trapped within the gel matrix, the presence of which has been verified in both aerogels and xerogels by ^{13}C CP/MAS NMR. Moreover, the significant volume loss noted in xerogel formation (relative to the wet gel and aerogel) suggests that the total pore volume of the xerogel must necessarily be a fraction of that available in the aerogel. Thus, we conclude that the xerogel drying results in a collapse of the inorganic framework that is only arrested by the presence of an organic fraction within the pores; the pores, which are clearly evident in TEM micrographs (Figure 1), are small and occluded (although not impermeable to gas adsorption). Aerogels, on the other hand, have free void space even though they also encompass a significant amount of organic; the soft-matter phase is insufficient to occlude the pores due to their larger size and fraction.

Conclusions

The porosity of CdS aerogels and xerogels prepared via sol-gel methods was evaluated using nitrogen sorption and

continuous flow HP ^{129}Xe NMR methods. Although both methods give information on pore size, the nitrogen physisorption measurements only provide a snapshot of the porosity characteristics and reflect those characteristics at low temperatures. In contrast, the NMR method gives information on pore hierarchy over a range of temperatures as well as the dynamics of Xe within the gel materials. Both nitrogen sorption and ^{129}Xe NMR data showed the presence of mesopores in the aerogel samples, with the BJH modeling of the nitrogen sorption isotherm showing a wide distribution of pores, the majority of which range from 5 to 90 nm, whereas ^{129}Xe NMR predicted two pore environments based on chemical shifts, both mesoporous. Moreover, 2-D EXSY NMR provided evidence of interconnectivity of the two pore environments based on the exchange of Xe gas between the pores, with one pore apparently acting as a pathway to the other. In contrast, for the xerogel counterpart, no meaningful data were obtained from nitrogen sorption isotherms and ^{13}C CPMAS NMR and TGA data suggested that a significantly higher percentage of residual organic groups remained in the air-dried xerogels, which likely occupied space and acted as a dynamic barrier (transport assisted via chain motion at higher temperatures) to any void volume that may otherwise have existed. Indeed, the ^{129}Xe chemical shift and changes in the chemical shift as a function of temperature in the case of the CdS xerogels were consistent with what has been observed for Xe dissolved in organic polymers, in the present case, most likely dissolution in residual AOT surfactant. These data suggest that better washing protocols are needed to improve accessibility to the pore structure of CdS dried gels, particularly for xerogels, where the surface area is known to be small even when the pores are not completely occluded by organics.

The presence of an interconnected mesopore and nanomatter architecture, wherein the "matter" is composed of native semiconducting materials (in this case, CdS, in lieu of the insulating SiO_2 matrix of a conventional aerogel), makes these materials uniquely suited to applications involving small molecule transport and photon-assisted or responsive processes, such as photocatalysis and optical sensing. The applicability of these materials to such processes is currently under investigation.

Acknowledgment. S.L.B. and K.K.K. acknowledge financial support from the NSF (DMR-0094273); the donors of the Petroleum Research Fund, Administered by the American Chemical Society; and the Wayne State University Institute of Manufacturing Research. Electron microscopy was acquired in the WSU Central Instrumentation Facility on a JEOL 2010 FasTEM purchased under NSF Grant No. DMR-0216084.

Supporting Information Available: Powder X-ray diffraction and ^{19}F MAS NMR spectra of a CdS aerogel and xerogel. This material is available free of charge via the Internet at <http://pubs.acs.org>.

References and Notes

- Hüsing, N.; Schubert, U. *Angew. Chem., Int. Ed.* **1998**, *37*, 22–45.
- Pierre, A. C.; Pajonk, G. M. *Chem. Rev.* **2002**, *102*, 4243–4265.
- Mohanan, J. L.; Arachchige, I. U.; Brock, S. L. *Science* **2005**, *307*, 397–400.
- Mohanan, J. L.; Brock, S. L. *J. Non-Cryst. Solids* **2004**, *350*, 1–8.
- Arachchige, I. U.; Brock, S. L. *J. Am. Chem. Soc.* **2006**, *128*, 7964–7971.
- Arachchige, I. U.; Brock, S. L. *J. Am. Chem. Soc.* **2007**, *129*, 1840–1841.
- Arachchige, I. U.; Brock, S. L. *Acc. Chem. Res.* **2007**, *40*, 801–809.
- Arachchige, I. U.; Mohanan, J. L.; Brock, S. L. *Chem. Mater.* **2005**, *17*, 6644–6650.
- Yu, H.; Bellair, R.; Kannan, R. M.; Brock, S. L. *J. Am. Chem. Soc.* **2008**, *130*, 5054–5055.
- Yu, H.; Brock, S. L. *ACS Nano* **2008**, *2*, 1563–1570.
- Brock, S. L.; Arachchige, I. U.; Kalebaila, K. K. *Comments Inorg. Chem.* **2006**, *27*, 1–24.
- Grasso, C.; Nanu, M.; Goossens, A.; Burgelman, M. *Thin Solid Films* **2005**, *480*, 87–91.
- Zhang, L.; Jiang, F. D.; Feng, J. Y. *Sol. Energy Mater. Sol. Cells* **2003**, *80*, 483–490.
- Seddon, A. B. *J. Non-Cryst. Solids* **1995**, *184*, 44–50.
- Kumta, P. N.; Risbud, S. H. *Mater. Sci. Eng., B* **1993**, *B18*, 260–268.
- Vassilev, V.; Boycheva, S.; Popov, C.; Petkov, P.; Alijehmani, L.; Monchev, B.; Kolev, K. *J. Non-Cryst. Solids* **2005**, *351*, 299–303.
- Wang, Y.; Mitkova, M.; Georgiev, D. G.; Mamedov, S.; Boolchand, P. *J. Non-Cryst. Solids* **2003**, *15*, 1573–1584.
- Sargent, E. H. *Adv. Mater.* **2005**, *17*, 515–522.
- Kim, S.; Lim, Y. T.; Soltész, E. G.; De Grand, A. M.; Lee, J.; Nakayama, A.; Parker, J. A.; Mihaljevic, T.; Laurence, R. G.; Dor, D. M.; Cohn, L. H.; Bawendi, M. G.; Frangioni, J. V. *Nat. Biotechnol.* **2004**, *22*, 969–976.
- Fraas, L. M.; Avery, J. E.; Huang, H. X.; Martinelli, R. U. *Semicond. Sci. Technol.* **2003**, *18*, S165–S173.
- Armatas, G. S.; Kanatzidis, M. G. *Nat. Mater.* **2009**, *8*, 217–222.
- Bag, S.; Trikalitis, P. N.; Chupas, P. J.; Armatas, G. S.; Kanatzidis, M. G. *Science* **2007**, *317*, 490–493.
- Telkki, V.-V.; Lounila, J.; Jokisaari, J. *J. Phys. Chem. B* **2005**, *109*, 24343–24351.
- Ripmeester, J. A. *J. Am. Chem. Soc.* **1982**, *104*, 289–290.
- Ito, T.; Fraissard, J. *J. Chem. Phys.* **1982**, *76*, 5225–5229.
- Ratcliffe, C. I. *Annu. Rep. NMR Spectrosc.* **1998**, *36*, 123–220.
- Raftery, D.; Chmelka, B. F. *NMR* **1994**, *30*, 111.
- Moudrakovski, I. L.; Ratcliffe, C. I.; Ripmeester, J. A. *Appl. Magn. Reson.* **1996**, *10*, 559–574.
- Jameson, C. J.; Jameson, A. K.; Gerald, R. E., II; Lim, H. M. *J. Phys. Chem. B* **1997**, *101*, 8418–8437.
- Chen, Q. J.; Springuel-Huet, M. A.; Fraissard, J. *Chem. Phys. Lett.* **1989**, *159*, 117–121.
- Moudrakovski, I. L.; Ratcliffe, C. I.; Ripmeester, J. A. In *Zeolites: A Refined Tool for Designing Catalytic Sites*; Bonneviot, L., Kaliaguine, S., Eds.; Elsevier Science: New York, 1995.
- Ripmeester, J. A.; Ratcliffe, C. I. *J. Phys. Chem.* **1995**, *99*, 619–622.
- Morgan, D. R.; Stejskal, E. O.; Andradý, A. L. *Macromolecules* **1999**, *32*, 1897–1903.
- Suzuki, T.; Miyauchi, M.; Yoshimizu, H.; Tsujita, Y. *Polym. J.* **2001**, *33*, 934–938.
- Wang, Y.; Inglefield, P. T.; Jones, A. A. *J. Polym. Sci., Part B* **2002**, *40*, 1965–1974.
- Goleme, G.; Nagy, J. B.; Fonseca, A.; Algieri, C.; Yampolskii, Y. *Polymer* **2003**, *44*, 5039–5045.
- Sozzani, P.; Comotti, A.; Simonutti, R.; Meersmann, T.; Logan, J. W.; Pines, A. *Angew. Chem., Int. Ed.* **2000**, *39*, 2695–2698.
- Joers, J. M.; Fong, P. M.; Gore, J. C. *Phys. Med. Biol.* **2006**, *51*, N23–N30.
- Moudrakovski, I. L.; Ratcliffe, C. I.; Ripmeester, J. A.; Wang, L.-Q.; Exarhos, G. J.; Baumann, T. F.; Satcher, J. H. *J. Phys. Chem. B* **2005**, *109*, 11215–11222.
- Gregory, D. M.; Gerald II, R. E.; Botto, R. E. *J. Magn. Reson.* **1998**, *131*, 327–335.
- Abidi, N.; Deroide, B.; Zanchetta, J. V.; de Menorval, L. C.; d'Espinose, J. B. *J. Non-Cryst. Solids* **1998**, *231*, 49–57.
- Gacoin, T.; Malier, L.; Boilot, J.-P. *Chem. Mater.* **1997**, *9*, 1502–1504.
- Gacoin, T.; Malier, L.; Boilot, J.-P. *J. Mater. Chem.* **1997**, *7*, 859–860.
- Gacoin, T.; Malier, L.; Boilot, J.-P. *J. Sol-Gel Sci. Technol.* **1998**, *13*, 61–64.
- Webb, P. A.; Orr, C. *Analytical Methods in Fine Particle Technology*; Micromeritics Instrument Corp.: Norcross, GA, 1997.
- Moudrakovski, I. L.; Lang, S.; Ratcliffe, C. I.; Simard, B.; Santyr, G.; Ripmeester, J. A. *J. Magn. Reson.* **2000**, *144*, 372.
- Driehuys, B.; Cates, G. D.; Miron, E.; Sauer, K.; Walter, D. K.; Happer, W. *Appl. Phys. Lett.* **1996**, *69*, 1668.
- Larsen, R. G.; Shore, J. S.; Schmidt-Rohr, K.; Emsley, L.; Long, H.; Pines, A.; Janicke, M.; Chmelka, B. F. *Chem. Phys. Lett.* **1993**, *214*, 220–226.
- Kritzenberger, J.; Gaede, H. C.; Shore, J.; Pines, A. *J. Phys. Chem.* **1994**, *98*, 10173–10179.
- Moudrakovski, I. L.; Ratcliffe, C. I.; Ripmeester, J. A. *J. Am. Chem. Soc.* **1998**, *120*, 3123–3132.

- (51) Moudrakovski, I. L.; Ratcliffe, C. I.; Ripmeester, J. A. *Appl. Magn. Res.* **1995**, *8*, 385–399.
- (52) Zhu, X.; Moudrakovski, I. L.; Ripmeester, J. A. *Energy Fuels* **1997**, *11*, 245–246.
- (53) Kentgens, A. P. M.; Van Boxtel, H. A.; Verweel, R. J.; Veeman, W. S. *Macromolecules* **1991**, *24*, 3712–3714.
- (54) Terskikh, V. V.; Moudrakovski, I. L.; Mastikhin, V. M. *J. Chem. Soc., Faraday Trans.* **1993**, *89*, 4239–4243.
- (55) Terskikh, V. V.; Moudrakovski, I. L.; Breeze, S. R.; Lang, S.; Ratcliffe, C. I.; Ripmeester, J. A.; Sayari, A. *Langmuir* **2002**, *18*, 5653–5656.
- (56) Martin, C. A.; Magid, L. J. *J. Phys. Chem.* **1981**, *85*, 3938–3944.
- (57) Gregg, S. J.; Sing, K. S. W. *Adsorption, Surface Area and Porosity*; Academic Press: London, 1982.
- (58) Ripmeester, J. A.; Ratcliffe, C. I. *J. Phys. Chem.* **1990**, *94*, 7652–7656.
- (59) Bowers, C. R.; Pietrass, T.; Barash, E.; Pines, A.; Grubbs, R. K.; Alivisatos, A. P. *J. Phys. Chem.* **1994**, *98*, 9400–9404.
- (60) Harel, E.; Granwehr, J.; Seeley, J. A.; Pines, A. *Nat. Mater.* **2006**, *5*, 321–327.
- (61) Walton, J. H.; Miller, J. B.; Roland, C. M. *J. Polym. Sci., Part B* **1992**, *30*, 527–532.
- (62) Raftery, D.; Reven, L.; Long, H.; Pines, A. *J. Phys. Chem.* **1993**, *97*, 1649–1655.

JP103157T